Astroparticle Physics 34 (2011) 493–502

Contents lists available at ScienceDirect

Astroparticle Physics

journal homepage: www.elsevier.com/locate/astropart

Toward an understanding of thermal X-ray emission of pulsars

M. Yu, R.X. Xu *

School of Physics and State Key Laboratory of Nuclear Physics and Technology, Peking University, Beijing 100871, China

ARTICLE INFO

Article history:
Received 20 April 2010
Received in revised form 25 September 2010
Accepted 28 October 2010
Available online 12 November 2010

Keywords:
Pulsars
Neutron stars
Elementary particles

ABSTRACT

We present a theoretical model for the thermal X-ray emission properties and cooling behaviors of isolated pulsars, assuming that pulsars are solid quark stars. We calculate the heat capacity for such a quark star, including the component of the crystalline lattice and that of the extremely relativistic electron gas. The results show that the residual thermal energy cannot sustain the observed thermal X-ray luminosities seen in typical isolated X-ray pulsars. We conclude that other heating mechanisms must be in operation if the pulsars are in fact solid quark stars. Two possible heating mechanisms are explored. Firstly, for pulsars with little magnetospheric activities, accretion from the interstellar medium or from the material in the associated supernova remnants may power the observed thermal emission. In the propeller regime, a disk-accretion rate $\dot{M} \sim 1\%$ of the Eddington rate with an accretion onto the stellar surface at a rate of $\sim 0.1\%\dot{M}$ could explain the observed emission luminosities of the dim isolated neutron stars and the central compact objects. Secondly, for pulsars with significant magnetospheric activities, the pulsar spindown luminosities may have been as the sources of the thermal energy via reversing plasma current flows. A phenomenological study between pulsar bolometric X-ray luminosities and the spin energy loss rates presents the probable existence of a 1/2-law or a linear law, i.e. $L_{\rm bol}^{\infty} \propto \dot{E}^{1/2}$ or $L_{\rm bol}^{\infty} \propto \dot{E}$. This result together with the thermal properties of solid quark stars allow us to calculate the thermal evolution of such stars. Thermal evolution curves, or cooling curves, are calculated and compared with the 'temperature-age' data obtained from 17 active X-ray pulsars. It is shown that the bolometric X-ray observations of these sources are consistent with the solid quark star pulsar model.

1. Introduction

It is conventionally thought that the thermal X-ray components of neutron stars are originated from the initial residual heat when the stars cool [48], even before the discovery of Galactic X-ray sources and pulsars. However, we will focus on this old problem in the regime of quark stars since there is no clear observational evidence to rule out quark stars or neutron stars. We demonstrate in this paper that the observed thermal emission of isolated pulsars could be well understood in a solid quark star model.

The study of quark matter phases, both hot and cold, has been an interesting topic of research in recent years. In an astrophysical context, quark stars composed by cold quark matter have yet not been ruled out by the measured properties of pulsar-like compact stars [58]. It has recently been proposed that realistic quark matter in compact stars could exist in a solid state [21,31,38,55], either as a super-solid or as a normal solid [58]. The basic conjecture of normal solid quark matter is that de-confined quarks tend to form quark-clusters when the temperature and density are relatively low. Below a certain critical temperature, these clusters could be in periodic lattices immersed in a degenerate, extremely relativistic, electron gas. Note that even though quark matter is usually described as weakly coupled, the interaction between quarks and gluons in a quark-gluon plasma is still very strong [44]. It is this strong coupling that could cause the quarks to cluster and form a solid-like material.

In fact, various kinds of observations could put constraints on the state of the matter in a pulsar, and the cooling behavior is suggested since 1960s, even before the discovery of pulsars. Can contemporary observations of X-ray thermal emitting and cooling pulsars be understood in the proposed solid quark star (hereafter SQS) model? This is a question we try to answer in the paper, and we address that SQSs could not be ruled out by the thermal observations. Moreover, SQSs might provide an opportunity to evaluate pulsar moments of inertia, if the thermal emission is also powered by spin.

In this paper, we argue that contemporary observations of thermal X-ray emitting pulsars are consistent with the assumption that these sources are in fact SQSs. The present analysis and calculation will concentrate on the observational temperature range, i.e. a few hundreds of to a few tens of eV. Nonetheless, a phenomenological scenario for the whole thermal history of a strange quark star is also outlined, as described in Section 2.1. The stellar residual heat

* Corresponding author. Tel.: +86 10 62758631; fax: +86 10 62765031.
E-mail address: r.x.xu@pku.edu.cn (R.X. Xu).

0927-6505/$ - see front matter
doi:10.1016/j.astropartphys.2010.10.017

would be the first energy source supporting the X-ray bolometric luminosities of SQSs. Section 2.2 is involved on this topic, including both of the partial contributions of the lattices and the electrons. Other energy reservoirs could exist as the stellar heating processes. This will be discussed in Section 2.3, where different heating mechanisms are introduced, according to the different X-ray pulsar manifestations. In Section 3, we compare the observations and the predictions given by the SQS pulsar model. Our conclusions as well as further discussions are presented in Section 4.

2. The model

2.1. Cooling stages of a quark star

The cooling process of a quark star can be quite complicated to model when starting from the birth of the star. Theoretical uncertainties make it difficult to predict the exact temperatures where phase transitions occur. For illustrative purposes, we present the following scenario where cooling of a quark star takes place in approximately three stages (see Fig. 1). The first stage occurs just after the birth of the quark star if its initial temperature is much higher than $\sim 10^{11}$ K (10 MeV). The emission of neutrinos and photons will lead to fast cooling. Hence, the star quickly enters the second stage where de-confined quarks begin to form quark clusters. As the temperature drops further, the fluid solidifies and the star is said to enter the third cooling stage or the SQS phase. Here, quark clusters form periodic lattice structures (e.g. the bcc structure).

It is uncertain exactly how long the star will spend in each phase, or even if it will ever enter all three states. If the initial temperature is just around 10^{11} K or lower, Stage 1 may be short lived or even non-existent. The quark-gluon plasma could be strongly coupled at birth and quark-clusters could be present immediately after formation. It is even possible that the melting temperature of solid quark matter could be $\sim 10^{11}$ K or higher. Hence, a quark star would enter Stage 3 immediately.

The mechanisms for the emission of thermal photons and neutrinos in each specific stage would be quite different. A hot quark star (in Stages 1 or 2) would be a good radiator for thermal equilibrium photons with energy more than ~20 MeV [1]. Meanwhile, the intense release of thermal energy would stimulate the generation and radiation of electron–positron pairs from the hot bare quark surface. The annihilation of the electron–positron pairs would generate the emission of photons inversely, and this plasma could be optically thick enough to produce a black body spectrum [49]. The emission of neutrinos would be given rise to by the pair production process as well as the plasma process induced by the ultra-relativistic degenerate electron gas inside the star [23]. The basic URCA process would be another neutrino radiation component for Stage 1. When the star cools down and becomes solidified (in Stage 3), thermal equilibrium photons (usually soft X-ray) could also be emitted from the bare SQS surface as free electrons transit in the levels of the energy bands of solid quark matter [55]. The electron–phonon interaction as well as the interaction between electrons themselves might result in a metal-like spectrum. Zhang et al. [64] analyzed the spectrum of RX J1856 phenomenologically, and they did not conclude that there are significant differences between the metal-like spectrum and black body spectrum. Hence, a black body thermal spectrum would be a good approximation for SQSs.The neutrino emissivity of clustered quark matter is theoretically so far unknown. The pair production and the plasma process would also lead the neutrino cooling for SQSs, if the stars enter the Stage 3 at high temperatures, such as $\sim 10^{11}$ K. Nevertheless, in the observational low temperature range $\sim 10^6 - 10^5$ K, the neutrino luminosity would be low enough so that photon cooling would be the dominant process for SQSs.

In general, in the low temperature range ($\sim 10^6 - 10^5$ K) which is the case considered by the present paper, the SQSs cool down by losing thermal photons, and the sources of the energy that enable the thermal emission are firstly the residual thermal energy of the stars and secondly the energy input caused by the processes of stellar heating. The energy relation would then be described as

$$-\frac{dU}{dt} + L_{SH} = L_{bol}, \tag{1}$$

where L_{bol} is the stellar bolometric X-ray luminosity, $-dU/dt$ is the release rate of the stellar residual thermal energy, and L_{SH} is the luminosity of stellar heating.

2.2. Residual thermal energy of a SQS

Provided that the volume of a SQS is a constant, then the stellar residual thermal energy U_{SQS} would only be the function of the stellar temperature T_s

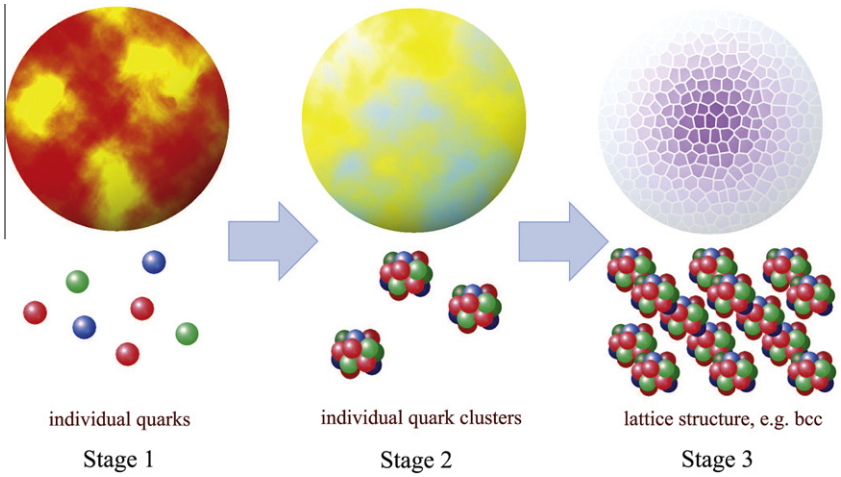

Fig. 1. Possible cooling stages of a quark star. *Stage 1*: individual quark phase. The temperature is high (>10 MeV) when the star is born, and the state of the star could be the fluid of individual quarks. *Stage 2*: individual quark cluster phase. As the temperature decreases, individual quarks tend to form quark clusters because of the strong coupling between them. The state of the star could then be the fluid of quark clusters. *Stage 3*: solid quark star phase. As the temperature drops to a melting temperature, the fluid of quark clusters tend to solidify to form periodic lattice structure, such as bcc structure.

$$U_{\rm SQS}(T_{\rm s}) = \int C_v \, {\rm d}T_{\rm s}, \tag{2}$$

where $T_{\rm s}$ is the value in the star's local reference frame. The heat capacity of the star C_v comprises of the partial contribution of the lattice structure $C_v^{\rm l}$ and that of the degenerate electrons $C_v^{\rm e}$, or $C_v = C_v^{\rm l} + C_v^{\rm e}$.

Following Debye elastic medium theory, the characteristic of the lattice heat capacity of solid quark matter could be evaluated by Debye temperature

$$\theta_D = \hbar\omega_D / k_{\rm B}, \tag{3}$$

where $\hbar$ is the reduced Planck constant, and $k_{\rm B}$ is the Boltzmann constant. ω_D is Debye cut-off frequency (i.e. the maximum frequency of the wave that could propagate in a medium), which equals Debye wave number $k_D = (6\pi^2 n_c)^{1/3}$(n_c is the number density of classical particles, or quark clusters for solid quark matter) times the average sound speed in the medium, i.e. $\omega_D = k_D \bar{c}_s$. For a SQS, the average sound speed could be the light speed approximately. A linear equation of state, extended to be used for a quark star, indicates that the pressure $p \sim \rho c^2$, where ρ is the mass density of a quark star and c is the speed of light. So an estimate could be $\bar{c}_s = \sqrt{{\rm d}p/{\rm d}\rho} \sim \sqrt{p/\rho} \sim \sqrt{\rho c^2/\rho} = c$. $n_c = 3\epsilon n_0/A$, where ϵ denotes the baryon number density of solid quark matter in the unit of n_0. n_0 is the baryon number density of normal nuclear matter and equals 0.17 fm^{-3}. We consider $\epsilon = 3-5$ could be the typical values for a SQS. Note that in the following calculation in this paper, we will adopt $\epsilon = 3$, since the variation of ϵ between 3 and 5 would not cause the results to vary in orders. A is the number of valence quarks in a quark cluster. We may expect that $A \sim 10$, since $A = 18$ if quark-α-like clusters are formed [37,55], and A could even be conjectured to be in the order of $\geqslant 10^2$. Debye temperature θ_D of a SQS is then $\sim 10^{12}$ K, which could be even higher than the temperature when a quark star is born. Hence, the heat capacity in the low-temperature limit or the temperature-cube law, is applicable for the lattice in the third stage, i.e.:

$$c_v^{\rm l} = \frac{12\pi^4}{5} k_{\rm B} \left(\frac{T_{\rm s}}{\theta_D}\right)^3, \tag{4}$$

where $c_v^{\rm l}$ is the heat capacity per classical particle (or quark cluster when referring to the solid quark matter) [50]. Thus $C_v^{\rm l} = N \cdot c_v^{\rm l}$, where N is the total number of clusters in a star.

For the stellar electron gas, those electrons distributed in the vicinity of the Fermi surface will contribute significant heat capacity. The electron heat capacity would be evaluated by

$$C_v^{\rm e} \sim N_{\rm e} \cdot \frac{k_{\rm B} T_{\rm s}}{E_F} \cdot k_{\rm B}, \tag{5}$$

where $N_{\rm e}$ is the number of electrons in a star, and E_F is the Fermi energy of the degenerate electron gas. In the extremely relativistic case, $E_F = \left(\frac{3n_{\rm e}h^3}{8\pi}\right)^{1/3} \cdot c$, in which $n_{\rm e}$ is the number density of electrons. According to the calculation using the bag model, $n_{\rm e}$ is typically chosen as one part in 10^5 of the baryon number density of strange quark matter [65]. In the three times nuclear density case, $n_{\rm e} \sim 5 \times 10^{33}$ cm^{-3}. E_F is hence in the order of $\sim$10 MeV. In Fig. 2, the heat capacities of these two components are plotted. As can be seen, the electron heat capacity is much larger than that of the lattice. Noting that it is really ambiguous about the melting temperature of a SQS, though we extended the calculation to 10 MeV.

We can now evaluate the cooling time scale for a SQS, if the star is only powered by its residual thermal energy. We choose the stellar mass of $1.4M_\odot$ as a typical case. We then have

$$-C_v \frac{{\rm d}T_{\rm s}}{{\rm d}t} = 4\pi R^2 \sigma T_{\rm s}^4 + L_v^{\rm pair} + L_v^{\rm plasma}, \tag{6}$$

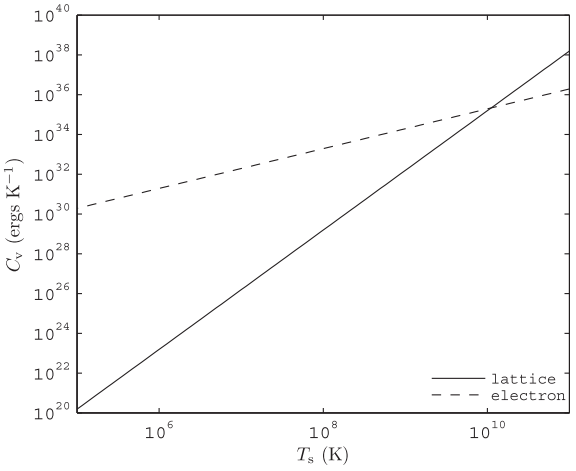

Fig. 2. Heat capacities of the lattice and electron components. The solid line is the result of the lattice structure, and the dashed line is that of the electron gas.

where R is the local stellar radius, σ is the Stefan–Boltzmann constant. On the right hand side of Eq. (6), the first energy loss component origins from the radiation of thermal photons, the second and the third terms are the neutrino luminosities induced by the pair production and the interior ultra-relativistic electrons, respectively. The calculation about these two neutrino luminosities refers to the analytic formulae given by Itoh et al. [23]. The concerning about the high temperature here makes the consideration on the neutrino cooling necessary. Although the actual neutrino emissivity of clustered quarks is hitherto unknown, these two components of neutrino emission could really take place for a SQS. Thus, one could obtain an upper bound on the residual-heat-powered cooling time scale for a SQS via Eq. (6). The calculation showed that a $1.4M_\odot$-SQS could only be sustained in $\sim$18 d, when it cools down from 10^{11} to 10^5 K. This would be the intrinsic distinction for SQSs from neutron stars. Neutron star cooling is mainly residual thermal energy powered, while thermal X-ray emission and cooling processes of SQSs could however be sustained by heating processes.

2.3. Stellar heating

Heating processes may play a significant role in the thermal evolution or the visibility of pulsars in the soft X-ray band. Pulsars with different magnetospheric properties may be undergoing different heating mechanisms.

2.3.1. Spin origin

Luminous nonthermal radiation and bright pulsar wind nebulae (PWNe), these observational manifestations may imply active magnetospheres. Strong star wind or relativistic particle flow would be ejected from the poles of such a pulsar. A certain amount of backflow of such plasma induce the stellar heating, or an energy input could take place at the polar caps and disperse to the bulk of the star [2,7,51,63]. The heat flow H could thus be

$$H \sim \frac{L_{\rm SH} - 4\pi r_{\rm p}^2 \sigma T_{\rm p}^4}{\pi r_{\rm p}^2} \sim \kappa \frac{T_{\rm p} - T_{\rm s}}{R}, \tag{7}$$

where $r_{\rm p} \approx R\sqrt{\Omega R/c}$ and $T_{\rm p}$ are the radius and the surface temperature of the polar caps in the local reference frame respectively. We adopted the one-dimensional approximation for the gradient of temperature, i.e. $\nabla T \sim (T_{\rm p} - T_{\rm s})/R$. The luminosity of the return-current stellar heating $L_{\rm SH}$ could be a function of the spin energy loss rate $\dot{E}$ and could generally be in the form of a power law. Moreover, a phenomenological study on the bolometric luminosity and $\dot{E}$ re-

veals that the power index could be 1/2 or 1, namely $L_{SH} = C\dot{E}^{1/2}$ or $L_{SH} = \eta\dot{E}$ (see Appendix A for details).

The metal-like interior of a SQS could imply that its thermal conductivity κ could be the sum of the partial components of phonons, electrons, and static impurities, or

$$\kappa = \kappa_{\rm p} + \kappa_{\rm e} + \kappa_{\rm imp}, \tag{8}$$

where the subscripts 'p', 'e', and 'imp' denote the partial components mentioned above, respectively. The electron thermal conductivity $\kappa_{\rm e}$ could be the dominant component for the metal-like solid material [11]. So phonon contribution $\kappa_{\rm p}$ would be neglected, and, as a preliminary model, we omit the partial component of static impurities. The electron thermal conductivity would be written as

$$\frac{1}{\kappa_{\rm e}} = \frac{1}{\kappa_{\rm ee}} + \frac{1}{\kappa_{\rm pe}}, \tag{9}$$

where $\kappa_{\rm ee}$ is the partial component contributed by the collision between electrons, while $\kappa_{\rm pe}$ is that contributed by the collision between phonons and electrons. For their analytic formulae, we refer to Flowers and Itoh [11] with assuming that the results remain hold for SQSs.

2.3.2. Accretion origin

Some pulsars, showing steady long-term soft X-ray fluxes, being inert in nonthermal emission, lacking the proves on the existences of the associated PWNe, (and sometimes) owning excesses of X-ray luminosities relative to the spin energy loss rates, could alternatively be inactive pulsar candidates. Due to their little magnetospheric manifestations, SQSs will not suggest the thermal X-ray radiation of these sources is of spin origin.

One possible way to understand the origin of the energy is the accretion in the *propeller* regime. In this regime, a shell of atmosphere of matter may form surrounding the star. Matter closing to the inner boundary of the shell may interact directly with the rotating stellar magnetosphere, as a result of which most of the matter will be expelled outward [27]. Nevertheless, a certain fraction of the accreting material, described by the accretion efficiency $\eta_{\rm acc}$, may diffuse starward and fall onto the surface of the star finally. In the propeller regime, the stellar magnetosphere radius or Alfvén radius $r_{\rm m}$ would be on one hand larger than its corotation radius $r_{\rm co}$, but is on the other hand somewhat smaller than the light cylinder radius $r_{\rm L}$, i.e.:

$$r_{\rm co} = \left(\frac{GM}{4\pi^2}\right)^{1/3} P^{2/3} \lesssim r_{\rm m} = \left(\frac{R^6 B_{\rm p}^2}{\dot{M}\sqrt{2GM}}\right)^{2/7} \lesssim r_{\rm L} = \frac{cP}{2\pi}, \tag{10}$$

where G is the gravitational constant, M, R, and $B_{\rm p}$ are the stellar mass, radius, and the magnetic strength at the poles, respectively. The accretion rate $\dot{M}$ could be scaled by Eddington accretion rate $\dot{M}_{\rm Edd}$; so μ could denote the accretion rate in this unit, i.e. $\dot{M} = \mu\dot{M}_{\rm Edd}$. During the accretion of the material which can reach the stellar surface eventually, the energy of gravitation would be released. Furthermore, when the two-flavor baryonic matter impact upon the surface of a SQS, it will burn into the three-flavor strange quark matter phase, and the latent heat of $\Delta\varepsilon \sim 10$–$\sim$100 MeV per baryon could be released in the phase transition [29]. The luminosity of stellar heating in this situation could then be

$$L_{\rm SH} = \frac{GM\cdot\eta_{\rm acc}\cdot\dot{M}}{R} + \Delta\varepsilon\frac{\eta_{\rm acc}\cdot\dot{M}}{m_{\rm p}}, \tag{11}$$

where $m_{\rm p}$ is the mass of a proton.

3. Observations versus expectations

We concentrate on those X-ray sources, which demonstrate significant thermal emission, own ordinary magnetic fields 10^{11-13} G, own comparatively young ages 10^{3-6} yrs, and have spins of a few tens of milliseconds to a few seconds. We mainly refer to the collation made by Yakovlev et al. [59] on cooling neutron stars, by Becker and Aschenbach [3] on X-ray pulsars, by Haberl [17] on X-ray dim isolated neutron stars (XDINs), and by Pavlov et al. [40] on central compact objects (CCOs). The sample exhibited in Table 1 thus comprises top 17 active pulsar candidates, 7 XDINs (Nos. 23–29) and 6 CCOs (Nos. 5 and 18–22). We note that the values of the surface temperatures adopted are determined by black body fits, according to the way that a SQS emits thermal photons. The XDINs and CCOs are considered to be magnetosphere-inactive pulsar candidates, since their quiescent manifestations on nonthermal radiation. CCOs, moreover, would only be seen in the soft X-ray band without the evidences on the existences of the associated PWNe. Additionally, we note that the emission of the energetic Crab pulsar is much likely to be overwhelmed by the nonthermal component originating from its luminous plerion, which hampers the detection to the stellar surface thermal radiation. As an estimate, we, however, adopted a 2σ upper limit to Crab's surface temperature and an inferred radius with assuming a 2 kpc distance between Crab and the earth [52]. RX J0822–4300, the central stellar remnant in Puppis A, used to be analyzed by Zavlin et al. [62] basing on the *ROSAT* observations in 1990s. They could not confirm whether the X-ray structures surrounding the star belong to the supernova remnant (SNR) or are induced by the probable active magnetosphere. Recent observations on it by *Chandra* and *XMM-Newton* telescopes, however, did not reveal the presence of the associated plerion, indicating an inert magnetosphere [22]. Because of the ambiguity of this source, we temporarily make it as one of the active source candidates.

Furthermore, we emphasize these X-ray sources that own measurable spin parameters in the $P-\dot{P}$ diagram (Fig. 3), by which a distribution of them can be read. Other 10 X-ray sources with constraints on the upper limits of their bolometric luminosities are also denoted in the diagram [3]. Besides the death line for a typical pulsar, those for low-mass SQSs are also indicated in the diagram. These death lines set boundaries of the 'graveyards' for pulsars with different mass [56]. The timing parameters are from ATNF Pulsar Catalog[1] [30], except for RX J0822–4300, which refers to Zavlin et al. [62].

For magnetosphere-active pulsar candidates, SQSs would suggest themselves to reproduce the cooling processes, while, for magnetosphere-inactive pulsar candidates, possible approaches to understand their current X-ray luminosities would also be proposed by SQSs. These two will be presented in Sections 3.1 and 3.2.

3.1. Cooling of active pulsar candidates

If two isotropic black body emission components – the hot component for polar caps and the warm one for the bulk of the star – are defined for SQSs, then the equation describing cooling processes would be written as (cf. Eq. (1))

$$L_{\rm SH} = 4\pi R^2\sigma T_{\rm s}^4 + 4\pi r_{\rm p}^2\sigma T_{\rm p}^4, \tag{12}$$

and the relation between $T_{\rm s}$ and $T_{\rm p}$ is given by Eq. (7). The luminosity of stellar heating $L_{\rm SH}$ could either follow the 1/2-law or the linear-law (see Appendix A). Cooling behaviors would thus be calculated by assuming SQSs rotate as orthogonal rotators and slow down as a result of magnetic dipole radiation with magnetic field

[1] www.atnf.csiro.au/research/pulsar/psrcat.

Table 1
Observational parameters on X-ray pulsars, including the surface temperature components $T^{\infty}_{s,1/2}$, the emission size components $R^{\infty}_{1/2}$ and the bolometric X-ray luminosity L^{∞}_{bol}. These are the values detected nearby the earth and fitted or analyzed by the black body model. Noting that (i) the age of 1E 1207.4–5209 (source No. 18) is adopted according to the estimate to the associated SNR, which is given by Haberl and Zavlin [16]; (ii) the ages of RBS 1223 and RX J0420.0–5022 are assessed by spindown ages in this work; (iii) the age limits of sources Nos. 1, 3–9, 11–12, 14–17, 23–24 are from Yakovlev et al. [59], while the rest ages are from the corresponding literatures listed in the last column; (iv) for 5 XDINs (Nos. 25–29), the black body parameters are obtained with an assumed distance of 100 pc, as a result of the lack or uncertain of their distances; (v) the spectral parameters for these sources are from the references listed in the last column: (1) Weisskopf et al. [52] (2) Zhu et al. [66] (3) Slane et al. [45] (4) Gonzalez et al. [12] (5) Hui and Becker [22] (6) Zavlin [60] (7) Halpern et al. [18] (8) Manzali et al. [32] (9) McGowan et al. [34] (10) Pavlov et al. [42] (11) McGowan et al. [33] (12) McGowan et al. [35] (13) Possenti et al. [43] (14) De Luca et al. [9] (15) Jackson and Halpern [24] (16) Zavlin and Pavlov [61] (17) Pavlov et al. [41] (18) De Luca et al. [8] (19) Chakrabarty et al. [6] (20) Kargaltsev et al. [26] (21) Gotthelf et al. [14] (22) Pavlov et al. [40] (23) Ho et al. [20] (24) Kaplan et al. [25] (25) Haberl [17] (26) Haberl et al. [15] (27) Haberl and Zavlin [16].

No.	Source	t (kyr)	$T^{\infty}_{s,1}$ (MK)	R^{∞}_{1} (km)	$T^{\infty}_{s,2}$ (MK)	R^{∞}_{2} (km)	L^{∞}_{bol} (10^{33} ergs s^{-1})	Refs.
1	PSR B0531+21 (Crab)	1	$\lesssim$1.85	$\gtrsim$ 15	–	–	$\sim$18.8	(1)
2	PSR J1811–1925 (in G11.2–0.3)	2	$\lesssim$1.74	–	–	–	–	(2)
3	PSR J0205+6449 (in 3C 58)	0.82–5.4	$\approx$1.7	$\approx$2.6	–	–	$\approx$0.44	(3)
4	PSR J1119–6127 (in G292.2–0.5)	$\sim$1.6	$2.4^{+0.3}_{-0.2}$	$3.4^{+1.8}_{-0.3}$	–	–	$2.0^{+2.5}_{-0.4}$	(4)
5	RX J0822–4300 (in Pup A)	2–5	$2.61^{+0.30}_{-0.26}$	$3.29^{+1.12}_{-0.74}$	$5.04^{+0.28}_{-0.20}$	$0.75^{+0.12}_{-0.15}$	$\approx$6.2	(5)
6	PSR J1357–6429	$\sim$7.3	1.7 ± 0.2	2.5 ± 0.5	–	–	$\approx$0.37	(6)
7	RX J0007.0+7303 (in CTA 1)	10–30	<0.66	$\approx$12	–	–	$<4.0 \times 10^{-2}$	(7)
8	PSR B0833–45 (Vela)	11–25	1.06 ± 0.03	$5.1^{+0.4}_{-0.3}$	$2.16^{+0.06}_{-0.07}$	$0.73^{+0.09}_{-0.07}$	$0.31^{+0.05}_{-0.04}$	(8)
9	PSR B1706–44 (in G343.1–02.3)	$\sim$17	$2.01^{+0.18}_{-0.20}$	$1.81^{+0.43}_{-0.29}$	–	–	$\approx$0.38	(9)
10	PSR B1823–13	$\sim$21	$1.61^{+0.10}_{-0.07}$	$\sim$2.5	–	–	$\approx$0.30	(10)
11	PSR J0538+2817 (in S147)	30 ± 4	$2.12^{+0.04}_{-0.03}$	1.68 ± 0.05	–	–	$\approx$0.46	(11)
12	PSR B2334+61 (in G114.3+0.3)	$\sim$41	1.62 ± 0.23	$1.66^{+0.59}_{-0.39}$	–	–	$\approx$0.11	(12)
13	PSR B1916+14	$\sim$88	$1.5^{+1.1}_{-0.6}$	$0.8^{-0.6}_{+5.2}$	–	–	$\approx$0.03	(2)
14	PSR B0656+14 (in Monogem Ring)	$\sim$110	0.91 ± 0.05	$\approx$14	1.9 ± 0.4	$\approx$0.8	$\approx$0.96	(13)
15	PSR J0633+1746 (Geminga)	$\sim$340	0.5 ± 0.01	8.6 ± 1.0	1.9 ± 0.3	0.04 ± 0.01	$\approx 3.2 \times 10^{-2}$	(14)
15′			0.482	$\approx$10	–	–		(15)
16	PSR B1055–52	$\sim$540	0.79 ± 0.03	$12.3^{+1.5}_{-0.7}$	1.79 ± 0.06	0.46 ± 0.06	$\approx$0.46	(14)
17	PSR J2043+2740	$\sim$1200	$\approx$0.9	$\approx$2	–	–	$\approx 2.0 \times 10^{-2}$	(16)
18	1E 1207.4–5209 (in PKS 1209–51/52)	$\sim 7^{+13}_{-4}$	1.90 ± 0.01	4.5 ± 0.1	3.70 ± 0.02	0.83 ± 0.02	$\approx$2.1	(17,18)
19	CXOU J232327.9+584842 (in Cas A)	0.3	6.14 ± 0.46	$0.41^{+0.08}_{-0.07}$	–	–	$1.7^{+1.6}_{-0.9}$	(19)
20	CXOU J085201.4–461753 (in G266.2–1.2)	<1.1	4.68 ± 0.06	0.28 ± 0.01	–	–	0.25 ± 0.02	(20)
21	PSR J1852+0040 (in Kes 79)	–	5.10 ± 3.48	0.9 ± 0.2	–	–	3.7 ± 0.9	(21)
22	PSR J1713–3949 (in G347.3–0.5)	–	4.4	2.4	–	–	15	(22)
23	RX J1856.5–3754	$\sim$500	$\approx$0.74	*5.0*	–	–	$\approx 5.2 \times 10^{-2}$	(23)
24	RX J0720.4–3125	$\sim$1300	$\approx$0.94	$\approx$6.1	–	–	$\approx$0.21	(24)
25	RBS 1223[a]	$\sim$400	1.04	0.8	–	–	5.1×10^{-3}	(25)
26	RX J0420.0–5022	$\sim$110	$0.66^{+0.29}_{-0.54}$	1.4	–	–	2.7×10^{-3}	(26)
27	RX J0806.4–4123	–	1.09 ± 0.01	$\approx$0.6	–	–	$\approx 3.6 \times 10^{-3}$	(27)
28	RX J1605.3+3249	–	1.07	$\approx$1.1	–	–	1.1×10^{-2}	(25)
29	RBS 1774[b]	–	1.04	$\approx$1.1	–	–	1.1×10^{-2}	(25)

[a] 1RXS J130848.6+212708.
[b] 1RXS J214303.7+065419.

strength at the poles of 10^{12} G. We provided a parameter space to fit the observational temperature-age data, and the comparison between the observations and expectations are shown in Fig. 4 (for 1/2-law case) and Fig. 5 (for linear-law case). Some pulsars demonstrate two black body components in their thermal spectra, e.g. Vela pulsar and the Three Musketeers, implying that the temperature inhomogeneity on these pulsars could be significant. We thus carried out a temperature-difference fit at the same time, as have been shown in the *right* panels in both Figs. 4 and 5. It is worthy of noting that, for Geminga, if the photon index of the power-law (PL) component is thawed when fitting its phase-resolved spectra, the entry of the hot black body component could not improve the fits remarkably, or it may even becomes an artifact. This may mean the fluctuation of the magnetospheric emission during a spin cycle might mislead the understanding on its X-ray spectra, as analyzed by Jackson and Halpern [24] and their results are denoted by No. 15′ in Table 1. If this situation holds, the surface temperature fluctuation on Geminga could be tiny so that undetectable. We, hence, set a rough upper limit to the temperature difference for Geminga by an order lower than its surface temperature, as denoted by 15′ in the 'temperature difference-age' figures.

The proposed relation between the rotational kinetic energy loss rate and the bolometric luminosity could inversely provide direct measurement to the moments of inertia of the active X-ray sources. The results are exhibited in Table 2 and could be understood in the SQS regime, especially low-mass SQSs (cf. the adoption of the coefficients C and η in Figs. 4 and 5). We note that for SQSs with $0.01M_{\odot}$, $0.1M_{\odot}$, $1.0M_{\odot}$ and $2.0M_{\odot}$, the moments of inertia I_{45} (i.e. values scaled by 10^{45} g cm^2) are $\sim 2.55 \times 10^{-4}$, $\sim$0.01, $\sim$0.55 and $\sim$1.74, respectively.

3.2. Thermal X-ray emission of inactive pulsar candidates

As has been discussed in Section 2.3.2, one probable energy source to be responsible for the soft X-ray emission of magnetosphere-inactive pulsar candidates lies in the accretion in the *propeller* regime. The accretion could be either to the interstellar medium or to the fallback disk. In this regime, however, the stellar magnetosphere radius could hardly be given, even though the sources' spindown rates are detectable. Because the spindown rate in this case would be dominated by the accretion behavior. Eq. (1) for this case could be specified as

$$L_{bol} = \frac{GM \cdot \eta_{acc} \cdot \dot{M}}{R} + \Delta\varepsilon \frac{\eta_{acc} \cdot \dot{M}}{m_p} \tag{13}$$

with considering Eq. (11) and the stellar residual thermal energy is too small to be taken into account. Table 3 lists the luminosities of

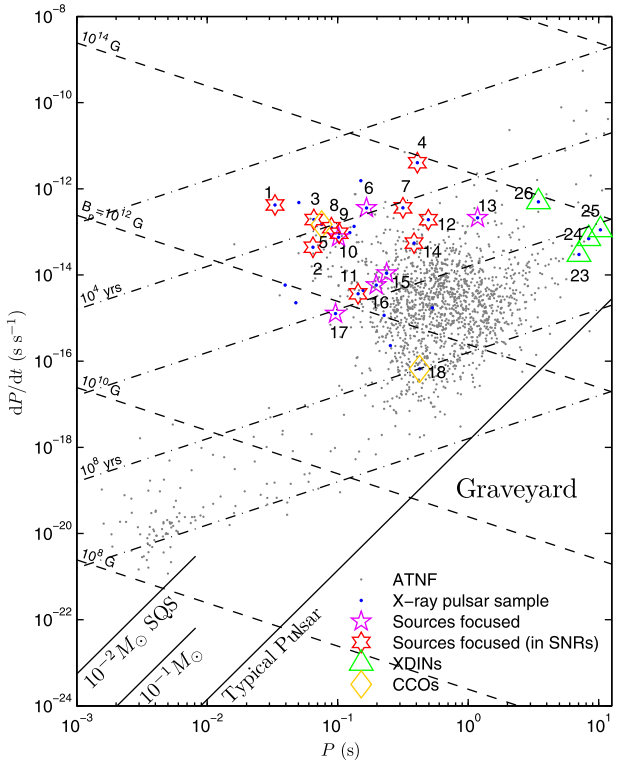

Fig. 3. $P-\dot{P}$ diagram for the X-ray pulsar sample. The solid lines indicate the death lines both for a typical pulsar (with mass of $1.4M_{\odot}$ and a radius of 10 km) and low-mass SQSs (with mass of $10^{-2}-10^{-1}M_{\odot}$), with surface magnetic field $B=10^{12}$ G and potential drop in open field line region $\delta\phi=10^{12}$ V. The death lines move up if decreasing B and/or increasing $\delta\phi$ [56]. The hexagonals indicate the focused sources associated with detectable supernova remnants (SNRs), while the pentagons indicate those which exhibit without evident SNRs. The triangles indicate 4 XDINs with measurable temporal parameters, and the diamonds mark the CCOs. The timing parameters for RX J0822–4300 are from Zavlin et al. [62], while the rest are from ATNF Pulsar Catalog (see footnote 1).

SQSs under the accretion scenario. It could be concluded that the sources' current observational thermal X-ray luminosities would be interpreted by considering the parameters μ, the accretion rate in the unit of that of Eddington, and $\eta_{\rm acc}$, the accretion efficiency, such as $\mu=0.01$, $\eta_{\rm acc}=0.001$.

4. Conclusions and discussions

We collate the thermal observations of 29 X-ray isolated pulsars and, in the SQS regime, for the magnetospherically active pulsar candidates, establish their cooling processes (Figs. 4 and 5), while for the magnetospherically inactive or dead pulsar candidates, interpret the X-ray luminosities under the accretion scenario (Table 3). Fitting to the thermal spectra for X-ray pulsars using the black body model often results in such small emission sizes that could naturally be interpreted by the SQS model. A recent study on the Cassiopeia A CCO shows that the fitted emission size is still significantly smaller than a typical neutron star radius, even if the hydrogen atmosphere model is employed in the fitting [39]. The uncertain estimates on the distances of pulsars may introduce considerable errors in the fitting about the X-ray source emission sizes. However, if these obtained emission radii can be trusted, SQSs, because of the possibility of being low-mass, could provide an approach to understand these observational manifestations. We note that for SQSs with mass of $0.01M_{\odot}$, $0.1M_{\odot}$ and $1M_{\odot}$, their radii are ~1.8, ~3.8 and ~8.3 km, respectively. On the other hand, a linkage between pulsar rotational kinetic energy loss rates and bolometric X-ray luminosities is explored by SQSs (see Appendix A), and the resulting estimates on pulsar moments of inertia is exhibited in Table 2.

We hence conclude that the phenomenological SQS pulsar model could not be ruled out by the thermal observations on X-ray isolated pulsars, though a full depiction on the thermal evolution for a quark star in all stages could hardly be given nowadays, as the lack of the physics in some extreme conditions (as has been discussed in Section 2.1). SQSs have significant distinguishable interiors with neutron stars, but the structures of the magnetosphere between these two pulsar models could be similar. Therefore, SQSs and neutron stars would have similar heating mechanisms, such as the bombardment by backflowing particles and the accretion to surrounding medium. However, a full comparison between SQSs and neutron stars including their cooling processes as well as the heating mechanisms has beyond the scope of this paper, and should be interesting and necessary in the future study.

The various performances of X-ray pulsars may indicate their current states or properties and imply their possible evolutionary history. In addition, if these X-ray sources are actually SQSs, the possible formation mechanism could be an interesting topic. We thus extend a discussion in Section 4.3.

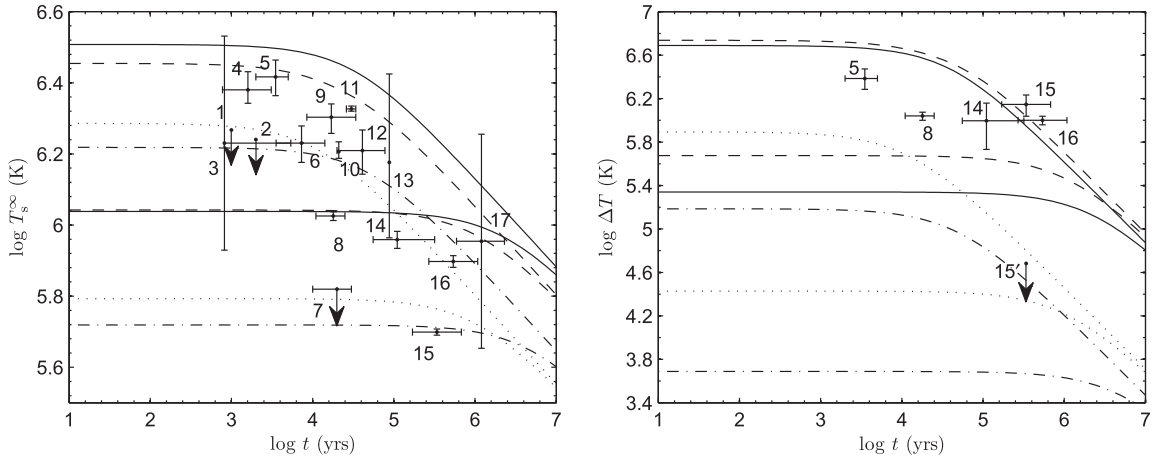

Fig. 4. *Left panel*: cooling curves for SQSs, if the 1/2-law between the bolometric luminosity and the spin energy loss rate holds. *Right panel*: corresponding temperature differences between the hot and warm components of SQSs, or $\Delta T=T_{\rm p}^{\infty}-T_{\rm s}^{\infty}$. The parameters in both panels: $M=0.1M_{\odot}$, $C=10^{16}$ (solid lines); $M=1.0M_{\odot}$, $C=10^{16}$ (dashed lines); $M=1.0M_{\odot}$, $C=10^{15}$ (dotted lines); $M=0.01M_{\odot}$, $C=10^{15}$ (dash-dot lines) (C is in the unit of ergs$^{1/2}$ s$^{-1/2}$). For two curves with same M and C, the upper one corresponds to an initial spin of 10 ms, while that of the lower one is 100 ms. Noting that the errors on the surface temperatures of PSRs J0205+6449 (No. 3) and J2043+2740 (No. 17) are not provided by the authors of the references, we then conservatively adopt them as deviating from the central values by a factor of 2.

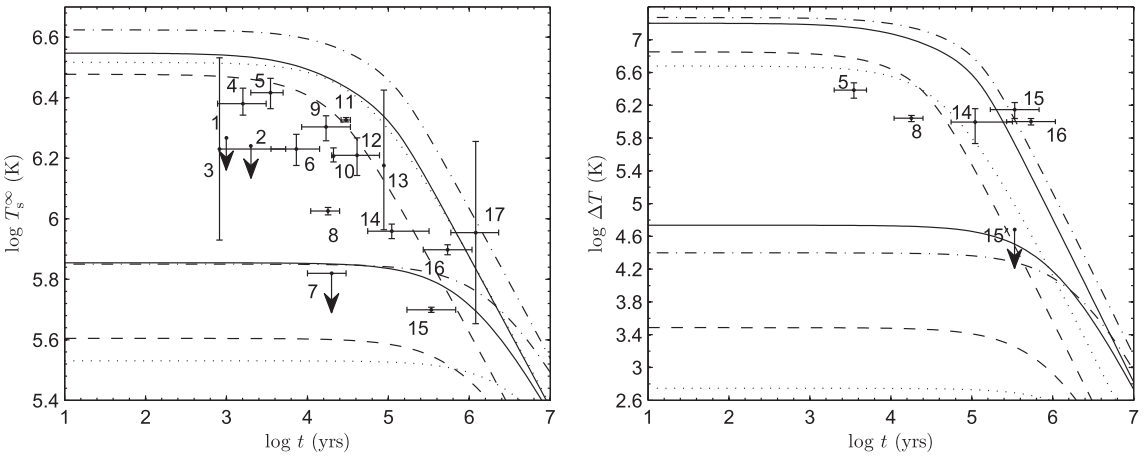

Fig. 5. *Left panel*: cooling curves for SQSs, if the linear-law holds. *Right panel*: temperature differences for this case. The parameters: $M = 1.0M_\odot$, $\eta = 0.01$ (solid lines); $M = 1.0M_\odot$, $\eta = 0.001$ (dashed lines); $M = 0.1M_\odot$, $\eta = 0.1$ (dash-dot lines); $M = 0.01M_\odot$, $\eta = 0.1$ (dotted lines). As in Fig. 4, for two curves with same M and η, the upper one corresponds to an initial spin of 10 ms, while the lower one 100 ms.

Table 2
The moments of inertia of active pulsar candidates suggested by SQSs. The 5th column lists the values derived by the 1/2-law, while the 6th column lists those obtained by the linear-law. The temporal parameters are from ATNF Pulsar Catalog (see footnote 1 for the website). For RX J0822–4300, we note that we adopt the spin parameters obtained by Zavlin et al. [62] basing on a 4.5 yr-span data set, though Hui and Becker [22] provided more recent values using a 0.5 yr-span data set.

No.	Source	ν (s^{-1})	$\dot{\nu}$ (s^{-2})	I_{45}[a] $\cdot C^2$ (ergs s^{-1})	$I_{45} \cdot \eta$
1	PSR B0531+21 (Crab)	30.225437	-3.862×10^{-10}	7.7×10^{29}	4.1×10^{-5}
2	PSR J1811–1925	15.463838	-1.052×10^{-11}	–	–
3	PSR J0205+6449	15.223856	-4.495×10^{-11}	5.8×10^{28}	4.6×10^{-5}
4	PSR J1119–6127	2.452508	-2.419×10^{-11}	1.7×10^{30}	8.5×10^{-4}
5	RX J0822–4300	13.2856716499(3)	$-2.6317(3) \times 10^{-11}$	2.7×10^{30}	2.8×10^{-4}
6	PSR J1357–6429	6.020168	-1.305×10^{-11}	4.4×10^{28}	1.2×10^{-4}
7	RX J0007.0+7303	3.165922	-3.623×10^{-12}	3.5×10^{27}	8.8×10^{-5}
8	PSR B0833–45 (Vela)	11.194650	-1.567×10^{-11}	1.4×10^{28}	4.5×10^{-5}
9	PSR B1706–44	9.759978	-8.857×10^{-12}	4.2×10^{28}	1.1×10^{-4}
10	PSR B1823–13	9.855532	-7.291×10^{-12}	3.2×10^{28}	1.1×10^{-4}
11	PSR J0538+2817	6.985276	-1.790×10^{-13}	4.3×10^{30}	9.3×10^{-3}
12	PSR B2334+61	2.018977	-7.816×10^{-13}	1.8×10^{29}	1.7×10^{-3}
13	PSR B1916+14	0.846723	-1.523×10^{-13}	1.8×10^{29}	5.9×10^{-3}
14	PSR B0656+14	2.598137	-3.713×10^{-13}	1.1×10^{31}	1.7×10^{-2}
15	PSR J0633+1746 (Geminga)	4.217640	-1.952×10^{-13}	3.2×10^{28}	9.9×10^{-4}
16	PSR B1055–52	5.073371	-1.501×10^{-13}	6.9×10^{30}	1.5×10^{-2}
17	PSR J2043+2740	10.402519	-1.374×10^{-13}	7.1×10^{27}	3.5×10^{-4}

[a] $I_{45} = I/(10^{45}\ \mathrm{g\ cm^2})$.

Table 3
The bolometric X-ray luminosity ($L_{\rm bol}$) contributed by the accretion of a SQS in the *propeller* regime. The corresponding accretion rates $\dot{M} = \mu\dot{M}_{\rm Edd}$ are also given. Noting that the values of luminosities are calculated by adopting $\Delta\varepsilon$, the latent heat per baryon during the phase transition, equals 100 MeV. In the propeller phase, the fraction of $\eta_{\rm acc}$ of the accreted matter diffuses starward and falls onto the stellar surface eventually.

Mass ($M_\odot$)	$\frac{\dot{M}}{\mu}$ ($10^{-9} M_\odot\ \mathrm{yr}^{-1}$)	$\frac{L_{\rm bol}}{\mu\cdot\eta_{\rm acc}}$ (10^{38} ergs s^{-1})
10^{-2}	2.7	1.7×10^{-1}
10^{-1}	5.7	4.7×10^{-1}
1.0	12.4	2.0

4.1. Spin-powered pulsars

Spin has always been a significant energy source for active pulsars, by which multiwave bands nonthermal radiation are driven, including those of the pulsar themselves as well as those of the surrounding plerions. Some phenomenological studies demonstrate certain regularities for such an active pulsar population. A brief summary is that the nonthermal X-ray luminosity and spin energy loss rate own a relation of $L_X = 10^{-3}\dot{E}$ [4], and the γ-ray luminosity is proportional to the square root of $\dot{E}$ or $L_\gamma \propto \dot{E}^{1/2}$ [46]. We, additionally, note that $V \propto \dot{E}^{1/2}$, where V is the potential drop along the open field region. Therefore, it seems that for such a population the more younger the larger $\dot{E}$ and V that a pulsar owns (cf. Fig. A.6, *bottom* panel) and the more luminous of the radiation in the hard X-ray and γ-ray bands.

Besides nonthermal emission, spin may also be an energy origin for pulsar thermal radiation as the relations of $L_{\rm bol}^\infty \propto \dot{E}^{1/2}$ or $L_{\rm bol}^\infty \sim 10^{-3}\dot{E}$ could exist observationally (see Appendix A for details). SQSs predominantly follow these relations to accomplish their cooling processes, since their residual thermal energy could be quite inadequate to sustain a long term X-ray thermal emission.

4.2. Accretion-powered pulsars

XDINs and CCOs could be representative populations of magnetosphere-inactive pulsars. Nevertheless, their energy origin that could power the X-ray emission is still an enigma. The bolometric luminosities of 1E 1207.4–5209, RX J1856.5–3754 and RX J0720.4–3125 exceed their spin energy loss rates by a factor of ~60, ~15 and ~45, respectively; they appear not to be powered by spins.

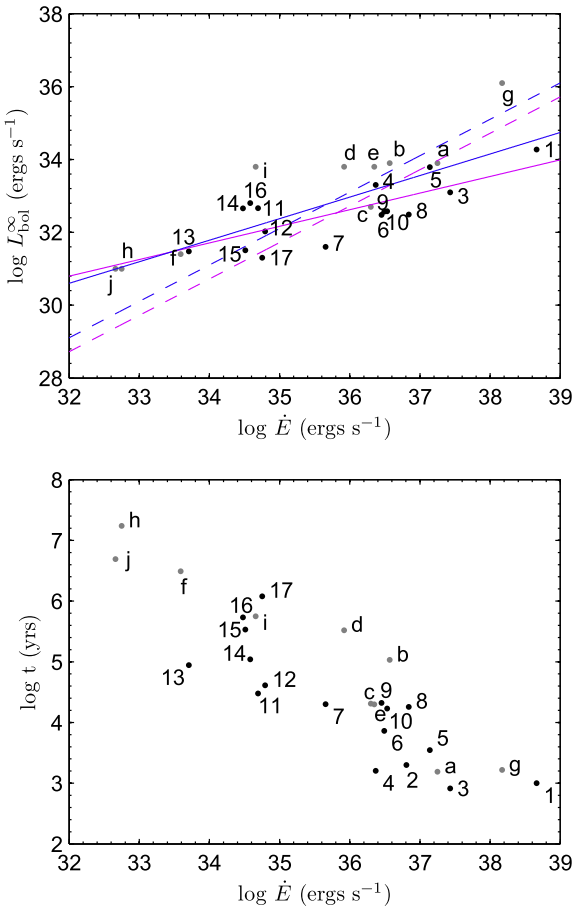

Fig. A.6. Functions $L_{\rm bol}^{\infty}(\dot{E})$ (*top* panel) and $t(\dot{E})$ (*bottom* panel) of active pulsar candidates. In the *top* panel, the fits are carried out both for Group A (including top 17 pulsars listed in Table 1; they are marked by dark points and their numbers) and Group B (including the members in Group A and the other 10 sources whose upper limits on the bolometric luminosities could be defined observationally; the 10 sources are marked by grey points and letters). Red lines are the fitted results for Group A, while blue lines are those for Group B. In both groups, solid lines provide the best fits to the data, while the dashed lines give the fits by freezing $p1$ at 1. We note that the 10 sources with upper limits on their bolometric luminosities defined are taken from Becker and Aschenbach [3], and they are a. B1509–58, b. B1951+32, c. B1046–58, d. B1259–63, e. B1800–21, f. B1929+10, g. B0540–69, h. B0950+08, i. B0355+54, j. B0823+26. (For interpretation of the references to colour in this figure legend, the reader is referred to the web version of this article.)

CCOs could be a group of weakly-magnetized and long-initial-period pulsars [13,41], because of which their potential drops along the open field lines could be much less than $\sim 10^{12}$ V, so that the primary plasma could not be fully accelerated, resulting in inactive magnetospheres. The black body fits to the thermal spectra of CCOs always result in extremely small emission sizes [40], implying the possible existence of low-mass SQSs. Therefore, the $\dot{E}$ of CCOs might be very low, so that effective magnetospheric emission and plerions could not be driven. CCOs could thus be the representatives of a group of natal inactive pulsars. Accretion to the fallback ejecta of the associated SNRs could power their soft X-ray luminosities, and this scenario have been mentioned by several authors (e.g. [6,10,19,26]).

XDINs, owning comparatively larger spindown ages and stronger magnetic fields, might be the descendants of magnetars. Considering similar properties between them [17,36], one could not exclude that XDINs are still being powered by the decaying magnetic fields. However, observations have revealed the probable existence of residual disks around such pulsars, and thus their radiation may be of accretion origin [28]. In this case, XDINs could be the evolved products of active pulsars, and thanks to the accretion so that they are still visible after their death. Most XDINs have absorption features in their spectra, being similar to those of CCOs. Hence, if they are really undergoing accretion in the propeller regime, their spindown rates $\dot{P}$ could then be of accretion origin rather than causing by the magnetic dipole braking. Thus their magnetic fields could be much lower than the values determined by canonical magnetic dipole radiation, since the absorption features could be electron cyclotron lines. Therefore, the common properties of absorption features between XDINs and CCOs could imply that XDINs might be older CCOs. XDINs and CCOs have not manifested themselves as radio pulsars, their radio-quiet demonstrations could be an intrinsic property rather than being of beaming origin, since they might be dead or natal inactive pulsars. So they could be grouped as radio-quiescent pulsars. For RX J0007.0+7303, an active pulsar candidate, its lack of radio signal could be the result of an unfavorable geometry, or its radio beam sweeps away from the earth as has been analyzed by Brazier and Johnston [5].

The similar thermal manifestations of accreting pulsars (e.g. XDINs and CCOs) and cooling pulsars may have caused a confusion about distinguishing between the two classes [47]. However, the activeness of the magnetosphere could provide a way to achieve an identification. If pulsars are in fact SQSs with rapid rotation, cooling pulsars are then likely to be undergoing the spindown-powered heating evolution, and multi-bands nonthermal emission originating from luminous magnetospheres and even PWNe will accompany such coolers during the processes. In contrast, accreting pulsars may have not demonstrated such characteristics observationally. In this context, the CCO in the SNR Cassiopeia A (source No. 19 in Table 1) should be an accretor because of the lack of PWN and nonthermal power-law component [39].

4.3. Formation of low-mass quark stars

Possible low-mass compact stars is a direct consequence of the suggestion that pulsars could be quark stars [56]. However, the probable existence of quark stars, spanning large mass range, could naturally raise such a question: how did these stars be created? Indeed, this could be another severe problem given by the observations. Being different from solar-mass quark stars (which could originate from core-collapse supernovae), low-mass quark stars could be the central remnants left by the detonation of the accretion-induced collapse (AIC) of white dwarfs (WDs) [57]. The combustion from the hadronic matter to the strange quark matter could be the engine of such an explosion. During this phase transition, as high as ~100 MeV per baryon could be released as the latent heat [29]. The combustion could hence be in such a high efficiency that %10 of the rest mass is liberated. For a WD approaching the Chandrasekhar limit, its mass and radius are $M_{\rm wd} \sim 1.4 M_{\odot}$, $R_{\rm wd} \sim 10^8$ cm, respectively. The gravitational energy is then $E_{\rm g} \sim (3/5) G M_{\rm wd}^2 / R_{\rm wd} \simeq 3 \times 10^{51}$ ergs. For a successful explosion of such a WD, the necessary mass of a quark star $M_{\rm qs,min}$ would hence be obtained by

$$0.1 M_{\rm qs,min} c^2 \simeq E_{\rm g}, \tag{14}$$

as $M_{\rm qs,min} \simeq 2 \times 10^{-2} M_{\odot}$. So, in this case, low-mass quark stars with a few tenth of or a few hundredth of solar mass could form, although one should be aware that the exact value of the quark star mass depends on the region where the detonation wave inside the WD can sweep though as well as the latent heat of the phase transition, which would be strongly model-dependent. These nascent quark stars would keep bare if they has not suffered massive Super-Eddington accretion [54]. An accreted ion (e.g. a proton) should gain enough kinetic energy to penetrate the Coulomb barrier

Table A.4
Fitting parameters for $L_{\rm bol}^{\infty} - \dot{E}$ data, which has been shown in Fig. A.6 (*top* panel).

Group	$p1$[a]	$p2$	Corr. Coef.[b]	χ_r^2 (d.o.f)[c]
A	0.4561 ± 0.2315	16.20 ± 8.30	–	0.3277(14)
	(1)	$-3.280^{+0.495}_{-0.494}$	0.7487	0.8607(15)
B	$0.5918^{+0.2045}_{-0.2046}$	$11.66^{+7.3100}_{-7.2990}$	–	0.6081(24)
	(1)	-2.896 ± 0.403	0.7730	0.9964(25)

[a] Values in the parenthesis are frozen during the fits. The errors are in 95% confidence level.
[b] Correlation coefficient of the data between bolometric luminosity and $\dot{E}$.
[c] Reduced χ^2, or χ^2 per degree of freedom (d.o.f).

of a quark star with mass $M_{\rm qs}$ and radius $R_{\rm qs}$, or $GM_{\rm qs}m_p/R_{\rm qs} > \mathcal{V}_{\rm q}$. The Coulomb barrier $\mathcal{V}_{\rm q}$ is model-dependent, which could varies from $\sim$20 MeV to even $\sim$0.2 MeV [53,57]. Considering $M_{\rm qs} = (4/3)\pi R_{\rm qs}^3\rho$ for low-mass quark stars, a mass lower-limit $M_{\rm qs,lim}$ would then be determined as

$$M_{\rm qs} > M_{\rm qs,lim} = \sqrt{\frac{3\mathcal{V}_{\rm q}^3}{4\pi G^3 m_p^3 \rho}} \simeq 4.6\times10^{-4}\mathcal{V}_{\rm q,1}^{3/2}\rho_3^{-1/2}M_{\odot}, \quad (15)$$

where the density $\rho = \rho_3 \times (3\rho_0)$, with ρ_0 the nuclear density, and $\mathcal{V}_{\rm q} = \mathcal{V}_{\rm q,1}$ MeV. Apart from the formation of the low-mass quark stars discussed here, other astrophysical processes, such as the collision between two strange stars, could also be the potential sources to give birth to the quark stars with smaller mass than that of the sun [1].

Acknowledgements

The authors are grateful to Prof. Fredrick Jenet for his valuable comments and advices, especially for his efforts on improving the English expression of this paper. The authors thank Mr. Weiwei Zhu for his detailed introduction to the observational situation about the sources PSR J1811–1925 and PSR B1916+14. The authors also thank the colleagues in the pulsar group of Peking University for the helpful discussion. This work is supported by NSFC (10778611,10973002), the National Basic Research Program of China (Grant 2009CB824800), and by LCWR (LHXZ200602).

Appendix A. Spin-powered thermal emission?

In the solid quark star (SQS) regime, cooling of magnetosphere-active pulsars depends predominantly on the stellar heating as a result of the lack of sufficient residual heat as has been analyzed in Section 2.2. The pulsar activity induced stellar heating would have intrinsically set up a linkage between the X-ray bolometric luminosity and the spin energy loss rate. We, hence, present here a phenomenological study on such a relation.

The sample of active pulsars firstly includes the top 17 sources listed in Table 1. Becker and Aschenbach [3] summarized X-ray pulsars, in which other 10 sources' upper limits on the bolometric luminosities could be defined. These 10 pulsars are meanwhile considered. Fig. A.6 (*top* panel) illustrates these sources' bolometric luminosities $L_{\rm bol}^{\infty}$ as a function of their spin energy loss rates $\dot{E}$, and Table A.4 lists the fitted parameters led by the function of

$$\log L_{\rm bol}^{\infty} = p1\cdot\log\dot{E} + p2. \quad (A.1)$$

The fits are carried out both only for the top 17 pulsars taken from Table 1 (as Group A) and for the whole sample with the other 10 sources included at the same time (as Group B). The best fits, moderate clearly, suggest a 1/2-law on the relation between pulsar bolometric X-ray luminosities and the spin energy loss rates, or

$$L_{\rm bol}^{\infty}(\dot{E}) = C\dot{E}^{1/2} \quad (A.2)$$

with a coefficient $C = 10^{p2}$ in the unit of ergs$^{1/2}$ s$^{-1/2}$. If $p1$ is fixed at 1, a linear-law is then implied, i.e.:

$$L_{\rm bol}^{\infty}(\dot{E}) = \eta\cdot\dot{E} \quad (A.3)$$

with a coefficient $\eta = 10^{p2}$, or η is the conversion efficiency. The fits obtain $\eta \sim 10^{-3}$, which is similar to the nonthermal X-ray case [4]. For the 1/2-law case, the conversion efficiency turns out to be the function of $\dot{E}$, which would be

$$\eta(\dot{E}) = \frac{C\dot{E}^{1/2}}{\dot{E}} = \frac{C}{\dot{E}^{1/2}}, \quad (A.4)$$

which could in turn, besides the fits, provide a reference to the value of the coefficient C by a natural constraint of $\eta(\dot{E}) < 1$. Taking B0823+26, the minimum $\dot{E}$ in our sample as an example, its C would be less than $\sim\sqrt{10^{32}} = 10^{16}$ ergs$^{1/2}$ s$^{-1/2}$. Additionally, we note here that we also present an age-$\dot{E}$ relation in the *bottom* panel of Fig. A.6, which illustrates a natural trend for spin-powered pulsars.

References

[1] C. Alcock, E. Farhi, A. Olinto, ApJ 310 (1986) 216.
[2] J. Arons, ApJ 248 (1981) 1099.
[3] W. Becker, B. Aschenbach, in: W. Becker, H. Lesch, J. Trümper (Eds.), WE-Heraeus Seminar on Neutron Stars, Pulsars and Supernova Remnants, Bad Honnef, 2002, p. 64.
[4] W. Becker, J. Trümper, A&A 326 (1997) 682.
[5] K.T.S. Brazier, S. Johnston, MNRAS 305 (1999) 671.
[6] D. Chakrabarty, M.J. Pivovaroff, L.E. Hernquist, J.S. Heyl, R. Narayan, ApJ 548 (2001) 800.
[7] A.F. Cheng, M.A. Ruderman, ApJ 214 (1977) 598.
[8] A. De Luca, S. Mereghetti, P.A. Caraveo, M. Moroni, R.P. Mignani, G.F. Bignami, A&A 418 (2004) 625.
[9] A. De Luca, P.A. Caraveo, S. Mereghetti, M. Negroni, G.F. Bignami, ApJ 623 (2005) 1051.
[10] R.A. Fesen, G.G. Pavlov, D. Sanwal, ApJ 636 (2006) 848.
[11] E. Flowers, N. Itoh, ApJ 250 (1981) 750.
[12] M.E. Gonzalez, V.M. Kaspi, F. Camilo, B.M. Gaensler, M.J. Pivovaroff, ApJ 630 (2005) 489.
[13] E.V. Gotthelf, J.P. Halpern, ApJ 664 (2007) L35.
[14] E.V. Gotthelf, J.P. Halpern, F.D. Seward, ApJ 627 (2005) 390.
[15] F. Haberl, W. Pietsch, C. Motch, A&A 351 (1999) L53.
[16] F. Haberl, V.E. Zavlin, A&A 391 (2002) 571.
[17] F. Haberl, Adv. Space Res. 33 (2004) 638.
[18] J.P. Halpern, E.V. Gotthelf, F. Camilo, D.J. Helfand, S.M. Ransom, ApJ 612 (2004) 398.
[19] J.P. Halpern, E.V. Gotthelf, F. Camilo, F.D. Seward, ApJ 665 (2007) 1304.
[20] W.C.G. Ho, D.L. Kaplan, P. Chang, M. Van Adelsberg, A.Y. Potekhin, MNRAS 375 (2007) 821.
[21] J. Horvath, Mod. Phys. Lett. A20 (2005) 2799.
[22] C.Y. Hui, W. Becker, A&A 454 (2006) 543.
[23] N. Itoh, T. Adachi, M. Nakagawa, Y. Kohyama, H. Munakata, ApJ 339 (1989) 354.
[24] M.S. Jackson, J.P. Halpern, ApJ 633 (2005) 1114.
[25] D.L. Kaplan, M.H. Van Kerkwijk, H.L. Marshall, B.A. Jacoby, S.R. Kulkarni, ApJ 590 (2003) 1008.
[26] O. Kargaltsev, G.G. Pavlov, D. Sanwal, G.P. Garmire, ApJ 580 (2002) 1060.
[27] V.M. Lipunov, Astrophysics of Neutron Stars, Springer-Verlag, Berlin, 1992.
[28] G. Lo Curto, R.P. Mignani, R. Perna, G.L. Israel, A&A 473 (2007) 539.
[29] J. Madsen, Hadrons in Dense Matter and Hadrosynthesis, vol. 162, Springer, Berlin, 1999.
[30] R.N. Manchester, G.B. Hobbs, A. Teoh, M. Hobbs, ApJ 129 (2005) 1993–2006.
[31] M. Mannarelli, K. Rajagopal, R. Sharma, Phys. Rev. D76 (2007) 4026.
[32] A. Manzali, A. De Luca, P.A. Caraveo, ApJ 669 (2007) 570.

[33] K.E. McGowan, J.A. Kennea, S. Zane, F.A. Córdova, M. Cropper, C. Ho, T. Sasseen, W.T. Vestrand, ApJ 591 (2003) 380.
[34] K.E. McGowan, S. Zane, M. Cropper, J.A. Kennea, F.A. Córdova, C. Ho, T. Sasseen, W.T. Vestrand, ApJ 600 (2004) 343.
[35] K.E. McGowan, S. Zane, M. Cropper, W.T. Vestrand, C. Ho, ApJ 639 (2006) 377.
[36] S. Mereghetti, ARAA 15 (2008) 225.
[37] F.C. Michel, Phys. Rev. Lett. 60 (1988) 677.
[38] B.J. Owen, Phys. Rev. Lett. 95 (2005) 211101.
[39] G.G. Pavlov, G.J.M. Luna, ApJ 703 (2009) 910.
[40] G.G. Pavlov, D. Sanwal, M.A. Teter, in: F. Camilo, B.M. Gaensler (Eds.), IAU Symposium on Young Neutron Stars and their Environments, San Francisco, vol. 218, 2004, p. 239.
[41] G.G. Pavlov, V.E. Zavlin, D. Sanwal, J. Trümper, ApJ 569 (2002) L95.
[42] G.G. Pavlov, O. Kargaltsev, W.F. Brisken, ApJ 675 (2008) 683.
[43] A. Possenti, S. Mereghetti, M. Colpi, A&A 313 (1996) 565.
[44] E.V. Shuryak, Prog. Part. Nucl. Phys. 62 (2009) 48.
[45] P. Slane, D.J. Helfand, E. Van de Swaluw, S.S. Murry, ApJ 616 (2004) 403.
[46] D.J. Thompson, A.K. Harding, W. Hermsen, M.P. Ulmer, in: C.D. Dermer, M.S. Strickman, J.D. Kurfess (Eds.), Proceedings of the Fourth Compton Symposium, AIP Conference Proceedings, vol. 410, AIP, New York, 1997, p. 39.
[47] A. Treves, R. Turolla, S. Zane, M. Colpi, PASP 112 (2000) 297.
[48] S. Tsuruta, Neutron Stars and Pulsars, Springer, Berlin, 2009.
[49] V.V. Usov, ApJ 550 (2001) L179.
[50] S.V. Vonsovsky, M.I. Katsnelson, Quantum Solid-State Physics, Springer-Verlag, Berlin, 1989.
[51] F.Y.-H. Wang, M.A. Ruderman, J.P. Halpern, T. Zhu, ApJ 498 (1998) 373.
[52] M.C. Weisskopf, S.L. O'Dell, F. Paerels, R.F. Elsner, W. Becker, A.F. Tennant, D.A. Swartz, ApJ 601 (2004) 1050.
[53] R.X. Xu, G.J. Qiao, Chin. Phys. Lett. 16 (1999) 778.
[54] R.X. Xu, ApJ 570 (2002) L65.
[55] R.X. Xu, ApJ 596 (2003) L59.
[56] R.X. Xu, MNRAS 356 (2005) 359.
[57] R.X. Xu, Int. J. Mod. Phys. D19 (2010) 1437.
[58] R.X. Xu, J. Phys. G: Nucl. Part. Phys. 36 (2009) 064010.
[59] D.G. Yakovlev, O.Y. Gnedin, A.D. Kaminker, A.Y. Potekhin, AIPC 983 (2008) 379.
[60] V.E. Zavlin, ApJ 665 (2007) L143.
[61] V.E. Zavlin, G.G. Pavlov, ApJ 616 (2004) 452.
[62] V.E. Zavlin, J. Trümper, G.G. Pavlov, ApJ 525 (1999) 959.
[63] B. Zhang, A.K. Harding, ApJ 532 (2000) 1150.
[64] X. Zhang, R.X. Xu, S.N. Zhang, in: F. Camilo, B.M. Gaensler (Eds.), IAU Symposium on Young Neutron Stars and their Environments, San Francisco, vol. 218, 2004, p. 303.
[65] W.W. Zhu, R.X. Xu, preprint, 2004. arXiv:astro-ph/0410265.
[66] W.W. Zhu, V.M. Kaspi, M.E. Gonzalez, A.G. Lyne, ApJ 704 (2009) 1321.